Materials and Design 114 (2017) 494–504

Contents lists available at ScienceDirect

Materials and Design

journal homepage: www.elsevier.com/locate/matdes

Fatigue crack growth rates for offshore wind monopile weldments in air and seawater: SLIC inter-laboratory test results

Ali Mehmanparast [a,*], Feargal Brennan [a], Isaac Tavares [b]

[a] Offshore Renewable Energy Engineering Centre, Cranfield University, Cranfield, Bedfordshire MK43 0AL, UK
[b] Centrica Renewable Energy Limited, Windsor, UK

HIGHLIGHTS

- Fatigue crack growth tests on BM and HAZ specimens have been conducted in air and free-corrosion seawater environments.
- A new shape function solution has been derived using Finite Element simulations and is presented in this paper.
- For both BM and HAZ materials, the FCG rate is on average around 2 times higher in seawater compared to air.
- In both air and seawater environments the mean curves for BM and HAZ fall close to each other.

GRAPHICAL ABSTRACT

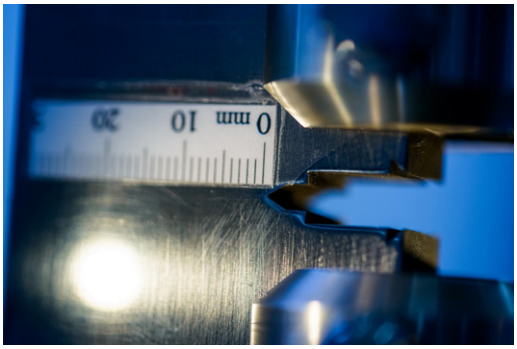

ARTICLE INFO

Article history:
Received 29 August 2016
Received in revised form 12 October 2016
Accepted 28 October 2016
Available online 2 November 2016

Keywords:
Fatigue crack growth
Monopile
Weldments
Offshore wind
HAZ
Base metal

ABSTRACT

The majority of fatigue crack growth (FCG) data sets available on steels in air and seawater environments are several decades old and may not be appropriate for structural integrity assessment of offshore wind turbine foundations, which are fabricated using contemporary materials and welding technologies. Therefore, the SLIC joint industry project was formed to investigate the fatigue crack initiation and growth behaviour in offshore wind welded steel foundations. The FCG test data from the SLIC inter-laboratory (round robin) test programme have been analysed using a new proposed shape function solution and the results are presented and discussed. The obtained FCG trends in air and seawater environments have been compared with the recommended trends available in standards. The Paris-law constants and ΔK_{th} values obtained from this programme can be used for defect assessment and remaining life prediction of offshore monopile weldments in air and seawater environments. The results from the SLIC project show that for a given value of ΔK the fatigue crack growth rate, da/dN, is on average around 2 times higher in seawater compared to air for the base metal and weldments. This factor of 2 in the seawater environment is almost half of the crack acceleration factor recommended by standards.

1. Introduction

Oil, coal and natural gas have powered the world energy demand for many years. Since the U.N. Climate Change Conference, COP21-Paris, a landmark agreement has been established with the aim of maintaining temperature rises well below 2 °C, thus slowing climate change. The use of clean renewable energy is encouraged globally to meet the targets to reduce greenhouse gas emissions. An efficient source of clean energy, which is increasingly becoming one of the preferred solutions to realising short-term and long-term energy ambitions in the world, is offshore wind due to its potential for large scale deployment. One of

* Corresponding author.
E-mail address: a.mehmanparast@cranfield.ac.uk (A. Mehmanparast).

http://dx.doi.org/10.1016/j.matdes.2016.10.070

Nomenclature

a	crack length
a_0	initial crack length
a_f	final crack length
da/dN	fatigue crack growth rate
B	specimen thickness
C	Paris-law coefficient
f	cyclic frequency
K	stress intensity factor
K_{max}	maximum stress intensity factor
K_{min}	minimum stress intensity factor
ΔK	stress intensity factor range
ΔK_{th}	stress intensity factor range threshold value
m	Paris-law exponent
N	number of cycle
P	applied load
P_{max}	maximum load level in cyclic test
P_{min}	minimum load level in cyclic test
R	the ratio of *Pmin* to *Pmin* in cyclic test (also known as load ratio)
R^2	coefficient of determination
W	specimen width
Y	shape function
α	crack length normalised by specimen width, a/W
σ	applied stress
σ_{max}	maximum stress in cyclic test
σ_{mean}	mean (average) stress in cyclic test
σ_{min}	minimum stress in cyclic test
$\Delta\sigma$	stress range
BFS	back face strain compliance
BM	base metal
C(T)	compact tension specimen geometry
ERF	environmental reduction factor
FE	finite element
HAZ	heat affected zone
LEFM	linear elastic fracture mechanics
PWHT	post-weld heat treatment
SD	standard deviation

the key challenges in the offshore wind industry is the life-cycle structural integrity design and assessment of the offshore wind turbine foundations, which are fabricated in much larger volumes, compared to other offshore industries such as Oil & Gas [1]. The majority of existing offshore wind turbine foundations are of thick-walled monopile type structures installed in shallow water. These structures, which are fabricated by welding relatively thick structural steel plates in longitudinal and circumferential directions, are subjected to extreme conditions in harsh offshore environments with the constant exertion of wave and wind forces causing both fatigue and corrosion damage. Therefore, the fatigue crack growth (FCG) behaviour of these offshore welded foundations needs to be accurately characterised in air and seawater environments in order to provide accurate remaining lifetime predictions and efficient inspection plans for offshore wind turbine structures. This can be done by performing laboratory scale FCG tests on standard fracture mechanics specimens made of parent material (also known as base metal (BM)) and weldments.

The experimental characterisation of FCG behaviour for various steels tested under different load ratios and frequencies in different environments can be found in [2–16]. Some more detailed studies on the near threshold FCG behaviour of steels in air and the marine environment are available in [8,9,16–20]. Using the FCG compendia available in the literature, empirical mean curves and conservative upper bound curves have been recommended for various metallic materials operating in different environments in BS7910 "British Standard Guide on methods for assessing the acceptability of flaws in fusion welded structures" [21]. The recommendations in BS7910 are for assessment of different metallic materials welded joints and BM operating in air and marine environments with and without cathodic protection. Much of the original research works, the results of which have been implemented in standards, are several decades old and were based on characteristics that were representative of typical Oil & Gas offshore structures [22]. In the intervening period, materials, fabrication technologies, inspection and design techniques have all evolved significantly. Therefore, it is vital to obtain a new fatigue data set on contemporary materials using representative manufacturing techniques employed in the offshore wind industry, and exposed to representative environments and loading conditions. This would support informed decisions concerning existing offshore wind structures and future developments in terms of design savings, construction, and operation. In order to achieve an improved understanding of fatigue in butt welded thick steel plates used in fabrication of offshore wind turbine monopile foundations, the SLIC (Structural Lifecycle Industry Collaboration) Joint Industry Project (JIP) was created. SLIC is a consortium of ten of the largest offshore wind operators (including Centrica, Dong Energy, EDF, EnBW, E.On, RWE, SSE, Statkraft, Statoil, Vattenfall) and The Crown Estate with the sponsorship of the UK's Department of Energy and Climate Change.

An important focus in the SLIC project is to undertake a programme of fatigue tests to establish the effects of offshore wind characteristics in the fatigue performance of welded steel foundations. Preliminary analysis suggested current guidance with respect to fatigue under free corrosion conditions is conservative, and significant design/operational benefit could be obtained through further testing. Therefore, an inter-laboratory (round robin) test programme was conducted to obtain comprehensive FCG data sets in air and in seawater, which can be used for defect assessment and remaining life prediction of thick-walled offshore monopile weldments. Seawater tests in this programme were carried out in a free-corrosion (i.e. no cathodic protection) environment at a characteristic dominant cyclic frequency typical of that experienced by offshore wind turbine structures. The details of these tests and the fatigue crack growth test results in air and seawater environments are presented in this paper.

2. Specimen design and manufacture

The material used in the fatigue crack growth testing work package in the SLIC project is EN-10225:01 S355G8 + M steel, which is widely used in the fabrication of offshore wind monopile structures. Multi pass butt-welding was conducted on double V-grooved plates with 90 mm thickness using the welding procedure employed to manufacture offshore wind monopile structures. No post-weld heat treatment (PWHT) was performed on the welded plates to replicate the real life conditions in monopiles. Compact tension, C(T), specimens were extracted from the 90 mm thick welded plates with the notch tip located in the BM and the heat affected zone (HAZ). C(T) specimens were extracted with crack planes perpendicular to the transverse axis and the crack propagation direction parallel to the normal (i.e. through thickness) axis, with respect to the welded plates. This orientation was selected to examine the through thickness crack growth behaviour of the circumferential weld regions in monopiles, where the cracks are most likely to initiate and grow under service conditions.

In order to locate the crack tip at the right place, particularly for HAZ specimens, reference sliced sections were extracted from the welded plates to explore the variation of the HAZ region in the welded plates. The reference sections were ground, polished and etched using 2% Nital solution to reveal the material microstructure in the weld region. An example of the etched surface of a weld section with the measured dimensions of the weld and HAZ regions is shown in Fig. 1. After revealing the material microstructure in sliced sections and measuring the

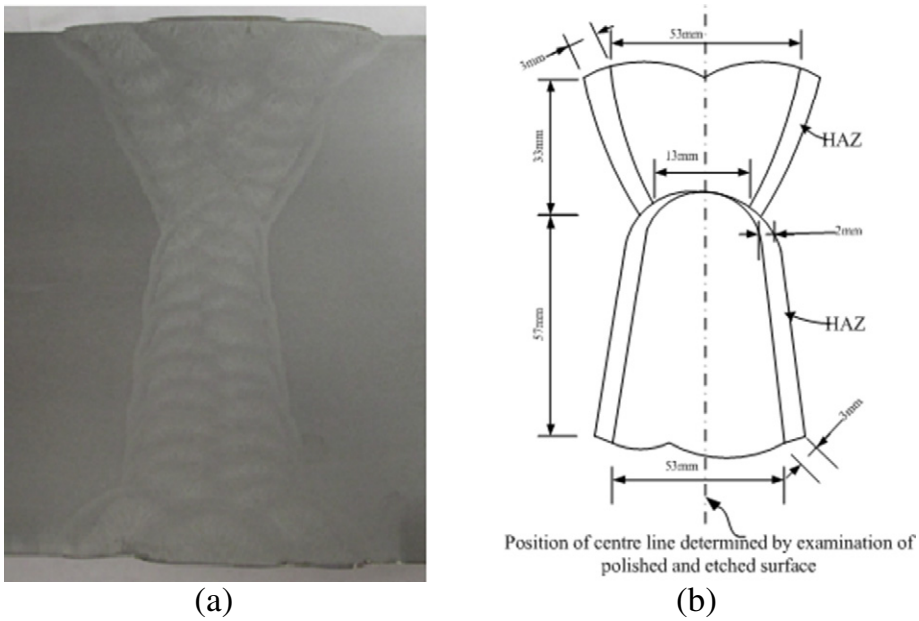

Fig. 1. (a) An example of a ground, polished and etched surface of the weld section (b) measured dimensions of the weld and HAZ regions.

dimensions of the weld region, specimens were extracted with the initial V-notch tip located at the centre of the HAZ region and within the base metal. A schematic illustration of the HAZ specimen orientation and the extraction location with respect to the weld region and also an example of the V-notch tip location in an etched HAZ specimen is shown in Fig. 2. Note that for the HAZ specimens, it was ensured that a sufficiently long and relatively straight HAZ region was located ahead of the V-notch tip to ensure that the crack growth occurred within the HAZ material.

C(T) specimen dimensions were designed following BS ISO 12108: 2012 standard for "Metallic materials; Fatigue testing - Fatigue crack growth method" [23]. The specimen dimensions for BM and HAZ C(T) specimens are summarised in Table 1. As seen in this table, the specimens width and thickness were approximately $W = 50$ mm and $B = 16$ mm in all C(T) specimens. 24 tests were performed in three Test Centres, which are referred to as A, B and C in this paper. The FCG specimens are labelled based on the material microstructure (i.e. BM and HAZ) and the Test Centre ID (i.e. A, B and C). For example, the BM specimens tested in Test Centre A are denoted BM-A1, and BM-A2. As noted in Table 1, 12 tests were performed on each material microstructure (i.e. BM and HAZ). Also shown in this table is that for each of the materials examined in this round robin test programme, half of the tests were performed in air whereas the other half were conducted in the simulated seawater environment.

3. Test set up procedure

3.1. Test machine preparation

FCG tests were performed in three independent Test Centres to examine the repeatability of the results. All tests centres were provided with the same test procedure and nominally identical specimens to make the results comparable. The tests were conducted both in air and free-corrosion seawater environments. It may be argued that the free-corrosion condition is not an offshore wind 'design condition', however there may be occasions where operators experience crack growth in unprotected regions (e.g. uncoated inner surface in some of the existing monopiles or where corrosion protection systems may have become damaged). The test machines used by different Test Centres were servo-hydraulic, purpose designed fatigue test machines with modern digital controllers and prepared following standards test methods [24–26]. Tests were conducted under load control and the machines therefore had both displacement control for set up purposes and load control for fatigue testing. Test Frame Rating was at least 100 kN to ensure adequate stiffness, and actuator stroke to be at least 75 mm. Checks were made to ensure adequate frame stiffness for the application. Before the commencement of any testing, the machine load cells were calibrated dynamically according to the relevant BS standard [27] to a level of 1.5 times the maximum test load. Prior to the commencement of the test programme, the test machine was checked for

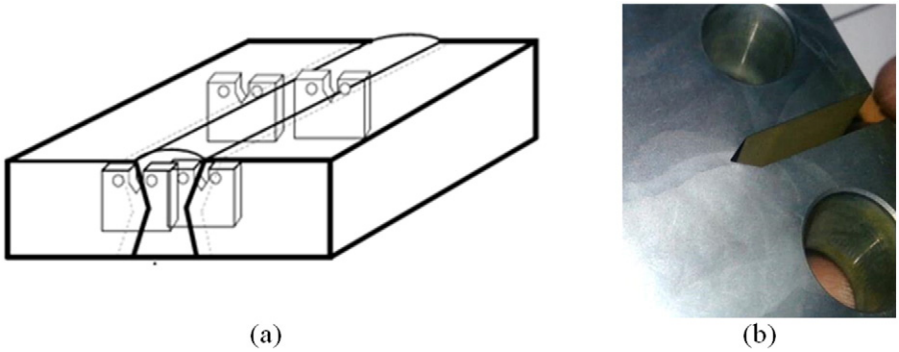

Fig. 2. (a) A schematic illustration of the HAZ specimen orientation and extraction location with respect to the weld region (b) an example of the V-notch tip location in an etched HAZ specimen.

Table 1
Specimen dimensions and loading conditions.

Test ID	Environment	W (mm)	B (mm)	a_0 (mm)	a_f (mm)	f (Hz)	R	P_{max} (kN)
BM-A1	Air	49.9	16.0	16.5	35.2	2.0	0.1	9.0
BM-A2	Air	49.9	16.0	14.8	28.8	2.0	0.1	6.7
BM-A3	Seawater	49.7	16.0	14.6	31.3	0.3	0.1	9.0
BM-A4	Seawater	49.7	16.0	14.3	31.5	0.3	0.1	9.0
BM-B1	Air	50.0	15.9	14.7	33.4	2.0	0.1	10.0
BM-B2	Air	50.0	15.9	14.5	35.0	2.0	0.1	10.0
BM-B3	Seawater	50.0	16.0	14.3	32.5	0.3	0.1	10.0
BM-B4	Seawater	50.1	15.9	14.0	31.0	0.3	0.1	10.0
BM-C1	Air	50.0	16.0	14.0	32.5	5.0	0.1	10.0
BM-C2	Air	50.0	16.0	14.0	32.5	2.0	0.1	10.0
BM-C3	Seawater	50.0	16.0	14.3	29.0	0.3	0.1	10.0
BM-C4	Seawater	50.0	16.0	14.3	30.1	0.3	0.1	10.0
HAZ-A1	Air	49.7	16.0	15.6	37.4	2.0	0.1	9.0
HAZ-A2	Air	49.6	16.0	15.1	31.5	2.0	0.1	9.0
HAZ-A3	Seawater	49.5	16.0	18.4	34.9	0.3	0.1	6.7
HAZ-A4	Seawater	49.8	16.0	16.0	31.5	0.3	0.1	9.0
HAZ-B1	Air	50.0	16.0	14.0	32.5	2.0	0.1	10.0
HAZ-B2	Air	50.0	16.0	14.3	32.0	2.0	0.1	10.0
HAZ-B3	Seawater	50.0	16.0	14.8	31.1	0.3	0.1	12.0
HAZ-B4	Seawater	50.1	16.0	14.0	30.5	0.3	0.1	10.0
HAZ-C1	Air	50.0	16.0	14.0	32.0	5.0	0.1	10.0
HAZ-C2	Air	50.0	16.0	14.0	32.0	5.0	0.1	10.0
HAZ-C3	Seawater	50.0	16.0	14.0	32.3	0.3	0.1	10.0
HAZ-C4	Seawater	50.0	16.0	14.0	32.3	0.3	0.1	10.0

alignment using a double pin-clevis arrangement as recommended in [23,28].

The test specimens were set up under position control taking care not to overload the specimens. The digital controller was programmed to ramp to the mean test load under load control and then to apply a constant amplitude sinusoidal wave form gently increasing to the test load range over five full cycles. The test load range was then applied without interruption until the end of the test. All specimens were pre-cracked to approximately 4 mm from the machined V-notch using the K-decreasing technique. The specimen pre-cracking was started with 12 kN maximum load and 1.2 kN minimum load, and these load levels were continuously decreased as the crack propagated. It was ensured that the highest load level in the pre-cracking stage did not exceed the maximum allowable load limit specified in the standard test method [23] and also the final K_{max} at the end of pre-cracking did not exceed the initial K_{max} for the main FCG tests. All specimens were pre-fatigue cracked in air at 10 Hz frequency.

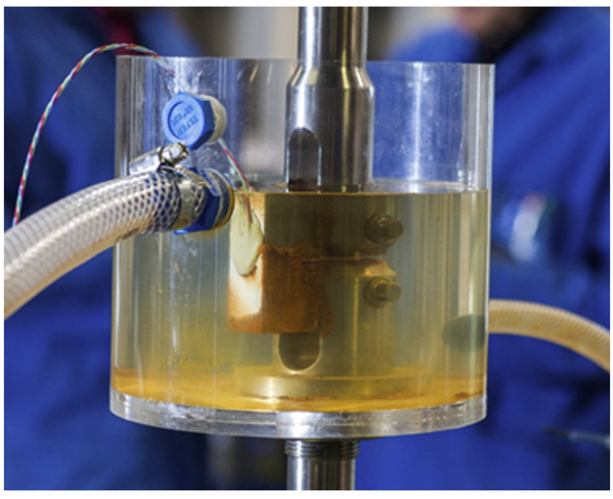

Fig. 3. An example of a seawater test set up.

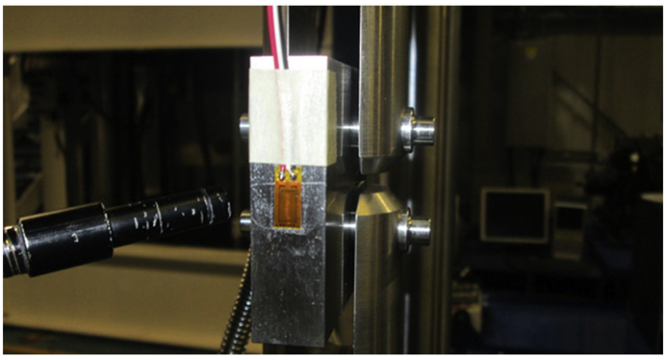

Fig. 4. Illustration of crack growth monitoring using back face strain measurements.

3.2. Seawater environmental cell

For seawater tests, an artificial non-biological seawater was prepared according to ASTM D1141 [29] and circulated through an environmental chamber at a rate of approximately 5 L/Min, at a temperature of 8–10 °C and a pH of 7.8–8.2. The entire test specimen was fully immersed at all times, and care was taken to eliminate any galvanic reaction between the test specimen and loading assembly as detailed in [30]. The reservoir size was at least 70 L in capacity. All seawater test specimens were soaked in the seawater for at least 48 h prior to the main test (i.e. after pre-cracking). An example of a seawater test set up is shown in Fig. 3.

3.3. Crack growth monitoring

An optical crack growth monitoring technique was employed to record instantaneous crack lengths during the pre-fatigue cracking stage and in the main FCG tests performed in air. For these tests, the crack growth was monitored on one side of the specimen using a high-resolution camera and on the other side using a travelling microscope. The average of crack lengths measured on both sides of the specimen was taken into consideration as the mean crack length value. For seawater tests, due to the difficulty in taking optical crack growth measurements through the environmental test chamber, the Back Face Strain (BFS) compliance method was used to estimate the crack lengths [31].

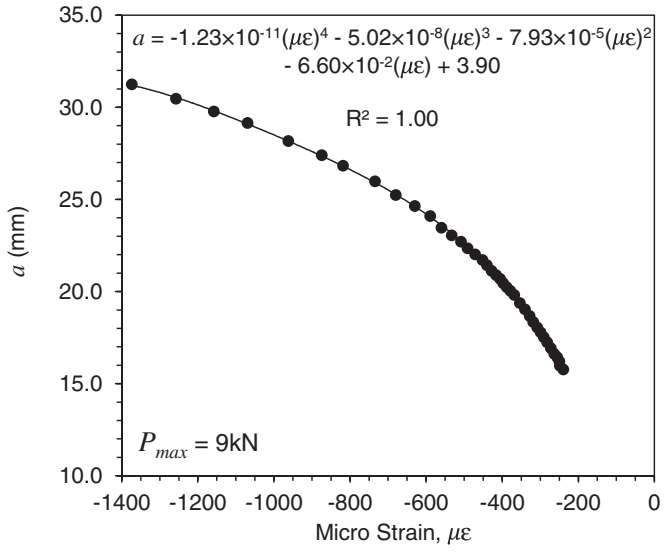

Fig. 5. An example of crack length correlation with back face strain measurements for the maximum applied load of Pmax = 9 kN.

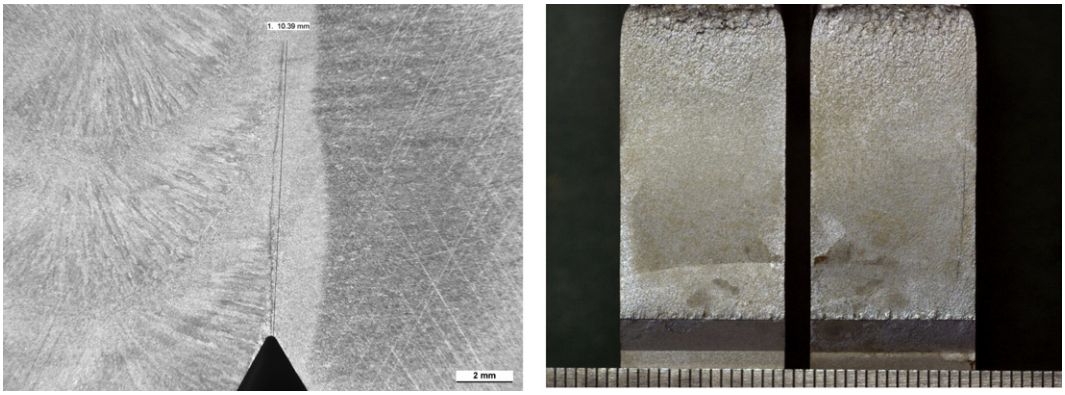

Fig. 6. (a) The crack path in a FCG test performed on HAZ specimen (b) Picture of a fracture surface.

In this technique, a Linear Electrical Resistance Strain Gauge was installed at the back face of each specimen (see Fig. 4) and the instantaneous crack lengths were calculated from the BFS measurements using a calibration function. An example of a calibration function, which correlates the crack length with BFS micro-strain values for a given loading condition, can be seen in Fig. 5. It should be noted that the BFS calibration function is dependent on the loading conditions and for FCG tests performed under varying load levels, different calibration functions must be developed and taken into consideration. For tests in seawater, to protect the strain gauge from the effect of corrosion, the strain gauge surfaces were coated with an appropriate coating material. The crack length measurements at the beginning (i.e. after pre-cracking), a_0, and end of FCG tests, a_f, for all specimens tested in this programme are summarised in Table 1.

3.4. Loading conditions

After pre-cracking, fatigue crack growth tests were performed at 0.3 Hz frequency for the tests in seawater and 2 and 5 Hz for the tests in air. A sinusoidal waveform with the load ratio of 0.1 was employed in all FCG tests in air and seawater. All air tests were performed at room temperature and seawater tests at 8–10 °C (typical of North Sea conditions). The cyclic frequency and loading conditions for each of the tests performed in this programme can be found in Table 1. Note that it has been shown by other researchers that the frequency has negligible effects on the FCG behaviour of steels in air [1,32,33]. However, FCG trends are known to be sensitive to cyclic frequency in a seawater environment [18]. It has been shown in the literature that offshore monopile wind turbine structures have a characteristic dominant cyclic structural response of around 0.3 Hz [34], therefore this frequency has been chosen for FCG tests in seawater.

Table 2
Simplified Paris-law constants recommended by BS7910 for da/dN in m/cycle and ΔK in MPa√m (the corresponding values for da/dN in mm/cycle and ΔK in N/mm$^{1.5}$ are shown in square brackets).

Material	Environment	C	m
BM	Air	1.65×10^{-11}	3.0
		$[5.21 \times 10^{-13}]$	[3.0]
BM	Seawater	7.27×10^{-11}	3.0
	(free-corrosion)	$[2.30 \times 10^{-12}]$	[3.0]
Welded joints	Air	4.91×10^{-12}	3.1
		$[1.10 \times 10^{-13}]$	[3.1]
Welded joints	Seawater	6.06×10^{-12}	3.5
	(free-corrosion)	$[3.41 \times 10^{-14}]$	[3.5]

3.5. Post-mortem analysis

Subsequent to test completion, the crack path in each specimen was observed under an optical microscope and the measured crack length on the outer surface of the specimen was compared to that measured on the fracture surface after specimen break open. Prior to specimen break open, the tested specimens were soaked in Liquid Nitrogen for a few minutes to minimise the sample deformation during the break open process. An example of the observed crack path in a FCG test on a HAZ specimen and a typical fracture surface observed subsequent to specimen break open are illustrated in Fig. 6.

3.6. Fatigue crack growth relations

Fatigue crack growth data are usually presented in the form of crack propagation rate (i.e. crack increment per cycle), da/dN, against the stress intensity factor range, ΔK, where K is the Linear Elastic Fracture Mechanics (LEFM) parameter, which can be defined as:

$$K = Y\sigma\sqrt{a} \tag{1}$$

where σ is the applied stress, a is the crack length and $Y(a/W)$ is a dimensionless shape function. The solution of $Y(a/W)$ for conventional fracture geometries can be found in fracture mechanics textbooks such as [35]. For a plane sided C(T) specimen the nominal stress can be defined as:

$$\sigma = \frac{P}{BW} \tag{2}$$

where P is the applied load, W is the specimen width and B is the specimen thickness. The solution of the shape function for a standard C(T) specimen is given in [23,36,37] as:

$$Y = \sqrt{1/\alpha}\left[\frac{(2+\alpha)(0.886+4.64\alpha-13.32\alpha^2+14.72\alpha^3-5.6\alpha^4)}{(1-\alpha)^{3/2}}\right] \tag{3}$$

where $\alpha = a/W$. Following the definition of K in Eq. (1), for a given crack length the change in stress intensity factor due to cyclic loading can be defined as:

$$\Delta K = K_{max} - K_{min} = \Delta\sigma Y\sqrt{a} \tag{4}$$

where the stress range $\Delta\sigma = (\sigma_{max} - \sigma_{min})$ is the difference between the stress corresponding to maximum load, Pmax, and minimum load, P_{min}. For a specimen subjected to a given cyclic loading condition, the main parameters, which influence the crack growth behaviour of the material, are the mean stress, σ_{mean}, and R-ratio (also known as load ratio)

Table 3
Two stage Paris-law constants recommended by BS7910 for *da*/*dN* in m/cycle and Δ*K* in MPa√m (the corresponding values for *da*/*dN* in mm/cycle and Δ*K* in N/mm$^{1.5}$ are shown in square brackets).

Material	Environment	*C* Stage A	*m* Stage A	*C* Stage B	*m* Stage B	Δ*K* transition from stage A to B	ΔK_{th}
BM	Air	2.10×10^{-17}	8.16	8.32×10^{-12}	2.88	11.5	4.7
		[1.21×10^{-26}]	[8.16]	[3.98×10^{-13}]	[2.88]	[363]	[149]
BM	Seawater (free-corrosion)	4.05×10^{-12}	3.42	1.13×10^{-8}	1.30	42.2	0
		[3.00×10^{-14}]	[3.42]	[1.27×10^{-7}]	[1.30]	[1336]	[0]
Welded joints	Air	9.38×10^{-13}	5.10	2.70×10^{-11}	2.88	4.5	2.0
		[2.10×10^{-17}]	[5.10]	[1.29×10^{-12}]	[2.88]	[144]	[63]
Welded joints	Seawater (free-corrosion)	2.32×10^{-11}	3.42	3.46×10^{-8}	1.11	23.6	0
		[1.72×10^{-13}]	[3.42]	[7.48×10^{-7}]	[1.11]	[748]	[0]

which can be defined as:

$$\sigma_{mean} = \frac{\sigma_{max} + \sigma_{min}}{2} \tag{5}$$

$$R = \frac{\sigma_{min}}{\sigma_{max}} = \frac{P_{min}}{P_{max}} = \frac{K_{min}}{K_{max}} \tag{6}$$

When *da*/*dN* is plotted against Δ*K* in log-log axes, there are generally three regions observed in a fatigue crack growth trend; (i) Region I (threshold) where ΔK_{th}, a minimum value of Δ*K* below which no fatigue crack propagation can be detected, is observed, (ii) Region II where a power-law relationship between *da*/*dN* and Δ*K* can be inferred, and (iii) Region III where an accelerating trend in FCG behaviour can be observed. For a metallic material subjected to cyclic loading conditions, the crack growth rate *da*/*dN* in the second FCG region, Region II, can be correlated with Δ*K* using the Paris-law equation [38], as:

$$\frac{da}{dN} = C\Delta K^m \tag{7}$$

where C and m are empirical power-law constants which can be found by a regression fit to the test data.

According to BS7910 standard [21], the FCG behaviour of a metallic material in Region II can be described using a simplified or 2-stage Paris-law. In simplified Paris-law relation a single fit is made to the data whereas in 2-stage Paris-law relation bi-linear fits, in log-log axes, are made to the data and two sets of Paris-law constants are reported for the earlier stage (i.e. Stage A) and the latter stage (i.e. Stage B). The simplified Paris-law constants for mean curves recommended by BS7910 [21] for BM and welded joints in air and free-corrosion seawater environments are summarised in Table 2. In this table, the power-law constants are given for *da*/*dN* in m/cycle and Δ*K* in MPa√m and the corresponding values for *da*/*dN* in mm/cycle and Δ*K* in N/mm$^{1.5}$ are shown in square brackets.

The 2-stage Paris-law constants recommended by BS7910 [21] for BM and welded joint mean curves in air and free-corrosion seawater environments are summarised in Table 3. The values given in this table are for *da*/*dN* in m/cycle and Δ*K* in MPa√m and the values for *da*/*dN* in mm/cycle and Δ*K* in N/mm$^{1.5}$ are shown in square brackets. Note that two sets of 2-stage Paris-law constants have been recommended by BS7910 for R-ratio of below and above 0.5. Having known that the applied R-ratio in the SLIC project was 0.1, the power-law constants for R < 0.5 from BS7910 have been extracted and tabulated in Table 3. Also included in this table are the Δ*K* transition points from Stage A to Stage B and also ΔK_{th} values recommended by BS7910 [21]. As seen in Table 3, BS7910 standard suggests taking ΔK_{th} as zero for BM and HAZ in the free-corrosion seawater environment. For air conditions, this standard suggests taking ΔK_{th} for welded joints as 2.0 MPa√m (i.e. 63 N/mm$^{1.5}$) and using the following equation to calculate ΔK_{th} for the BM.

$$\Delta K_{th} = 170 - 214R \text{ N/mm}^{1.5} \text{ for } 0 \le R < 0.5 \tag{8}$$

4. Fatigue crack growth results

Fatigue crack growth tests were performed in air and free-corrosion seawater environments using the loading conditions specified in Table 1. The crack lengths were measured as a function of the number of elapsed force cycles in all FCG tests in air and seawater. Using these raw data, the FCG rate, *da*/*dN*, was calculated using a 7-point incremental polynomial technique as recommended by BS and ASTM standard tests method for fatigue crack growth testing and analysis [23,37]. In the process of Δ*K* calculations for different FCG tests using the equations provided in standard test methods, it was noted that the initial normalised crack length, a_0/W, for the majority of the tests performed in this project was <0.45 (see Table 1). BS ISO 12108: 2012 [23] and ASTM E647 [37] standards suggest that for C(T) specimens with $0.2 \le a/W \le 1.0$ the shape function solutions can be calculated using Eq. (3). However, it was noted in a previous work [39] that for shallow cracks the shape function solutions for C(T) do not follow the trend provided by Eq. (3). Therefore, the shape function solutions for shallow cracks were evaluated in this work using numerical analyses and the new solutions were employed to analyse the FCG test data from the SLIC project. The new shape function solution and FCG trends obtained from tests performed on different material microstructures in air and seawater are presented and described next.

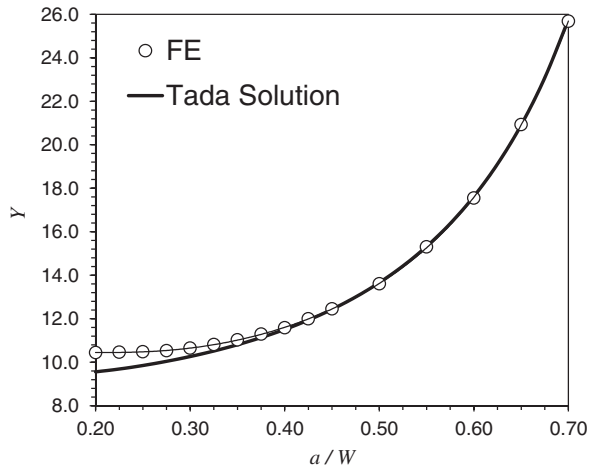

Fig. 7. Comparison of numerical solution of shape function with Tada solution.

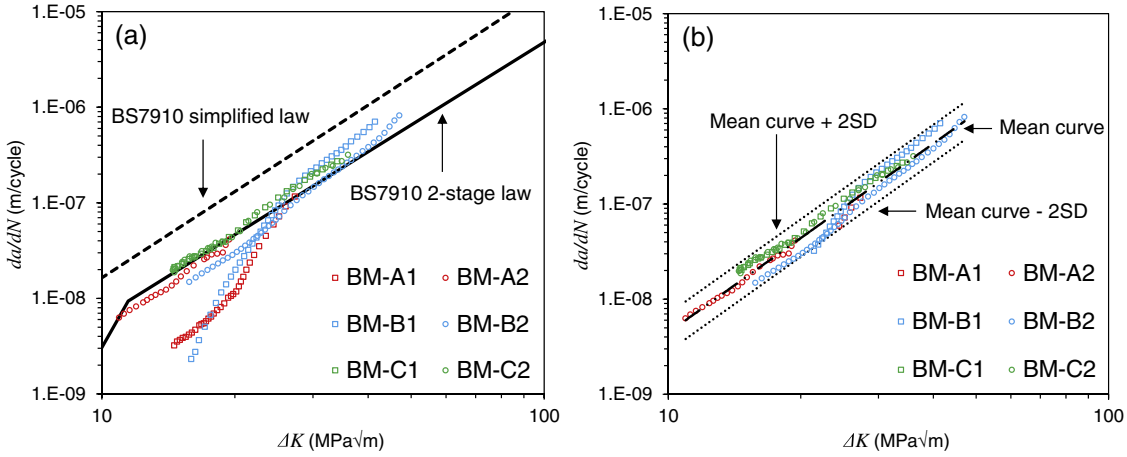

Fig. 8. FCG test data on BM in air (a) comparison with BS7910 recommended trends, (b) line of best fit made to the linear data points in log-log axes.

4.1. Numerical shape function solutions for shallow cracks

It has been suggested in [23,37,40] that Eq. (3), which is also known as the Tada solution, is valid for 0.2 ≤ a/W ≤ 1.0 in C(T) specimens. In this work, numerical simulations have been performed to investigate the accuracy of the suggested solutions for a wide range of crack lengths. Finite Element (FE) simulations were carried out on a C(T) specimen geometry using elastic material properties in ABAQUS software package [41] and the stress intensity factor, K, was numerically evaluated using the domain-integral technique (see [41]) by defining 40 contours around the crack tip. A single-node crack tip, surrounded by a focused mesh, was designed for this purpose. The numerical values of the shape function for $0.2 \le a/W \le 1.0$ have been calculated using Eq. (1) and compared with the Tada solution in Fig. 7. As seen in this figure, the percentage error encountered in the calculation of the shape function using the Tada solution rapidly increases as a/W decreases below 0.4. Therefore, a new shape function solution, which has been obtained from the line of best fit made to the numerical data points for the normalised crack length ranging from 0.2 to 0.7, is proposed for C(T) specimen geometry as:

$$Y = (-372.12\alpha^6 + 1628.60\alpha^5 - 2107.46\alpha^4 + 1304.65\alpha^3 - 391.20\alpha^2 + 54.81\alpha + 7.57) \quad (9)$$

4.2. Fatigue crack growth behaviour of the BM in air and seawater

The fatigue crack growth rate, da/dN, obtained from the tests performed on the BM in air and seawater is correlated with the stress intensity factor range, ΔK, and the results are shown in log-log axes in Fig. 8 and Fig. 9, respectively. The FCG data on the BM are compared with the simplified and 2-stage Paris-law trends recommended by BS7910 [21] (see Table 2 and Table 3) in Fig. 8(a) and Fig. 9(a). The mean fits to the linear data points, in log-log axes, and the upper bound/lower bound trends, obtained by calculating ±2 standard deviation (2SD), are exhibited in Fig. 8(b) and Fig. 9(b).

It can be seen in Fig. 8(a) that the first half of FCG data points for BM in air fall upon or below the 2-stage trend recommended by BS7910, however the latter half of the data points fall in between the simplified and 2-stage trends recommended by BS7910, tending towards the simplified trend. This figure suggests that for the stress intensity factor range of $10 < \Delta K < 50$ MPa√m, the simplified Paris-law recommended by BS7910 provides a conservative estimate of the BM FCG behaviour in air. Furthermore as seen in Fig. 8(a) some variation exists between the FCG behaviour of BM-A1 and BM-A2, obtained from Test Centre A, and also BM-B1 and BM-B2, obtained from Test Centre B, in the early stages of the FCG tests. This can be associated with material variability, which may influence the early stage FCG behaviour of the material. Although the obtained trends from BM-A1 and BM-B1 suggest that ΔK_{th} of the BM in air is approximately 15 MPa√m, it is evident from higher

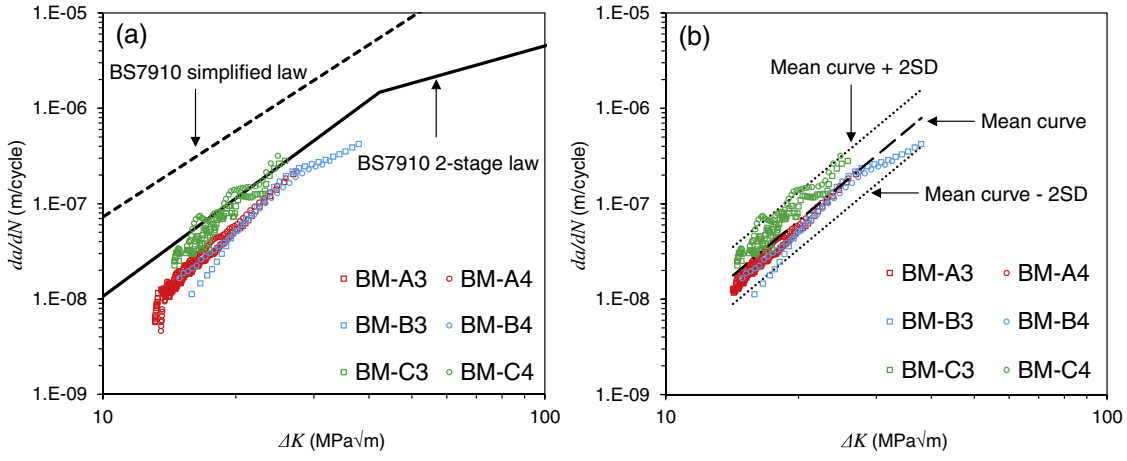

Fig. 9. FCG test data on BM in seawater (a) comparison with BS7910 recommended trends, (b) line of best fit made to the linear data points in log-log axes.

Table 4
Simplified Paris-law constants from SLIC test data (for da/dN in m/cycle and ΔK in MPa√m) using corrected shape function solutions.

Material	Environment	Mean curve			Mean + 2SD	
		C	m	R^2	C	m
BM	Air	2.25×10^{-12}	3.30	0.96	3.54×10^{-12}	3.30
BM	Seawater (free-corrosion)	6.25×10^{-13}	3.86	0.83	1.25×10^{-12}	3.86
HAZ	Air	2.16×10^{-13}	3.97	0.96	3.21×10^{-13}	3.97
HAZ	Seawater (free-corrosion)	4.67×10^{-12}	3.23	0.98	6.29×10^{-12}	3.23

FCG trends obtained from other specimens that $\Delta K_{th} = 15$ MPa√m cannot be taken as a conservative threshold value for BM in air. In order to work out the Paris-law constants for BM in air, the mean curve and the upper/lower bound trends (mean curve ± 2SD) were initially plotted based on those test data sets exhibiting predominantly linear behaviour, in log-log axes, for the range of ΔK examined (BM-A2, BM-B2, BM-C1 and BM-C2). Then the deviated data points from other test data sets (BM-A1 and BM-B1) which fell outside the upper and lower bound trends were removed. Finally, the remaining data points were re-analysed to work out the Paris-law and upper/lower bound trends that have been shown in Fig. 8(b). The Paris-law constants found from the "mean curve" and "mean curve ± 2SD" are summarised in Table 4. Moreover, the R^2 values for each trend line are reported in Table 4 to examine the accuracy of each fit made to the experimental data. It can be seen in Fig. 8(b) and Table 4 that assuming the same slope in the mean curve and upper/lower bound trends, the Paris-law coefficient and consequently the FCG rate at the upper bound trend is 1.6 times higher than the mean curve for BM in air.

Fig. 9(a) shows that the FCG data for BM in seawater fall upon or below the 2-stage law recommended by BS7910, indicating that the trend suggested in this standard provides a good estimate of FCG behaviour for BM in free-corrosion conditions. Also seen in this figure is that the FCG trends obtained from BM-B3 and BM-B4 specimens exhibit a reduced slope towards the end of the test. This slope reduction at higher values of ΔK is consistent with the BS7910 2-stage Paris-law trend recommendation, although this change in slope has occurred at a lower ΔK value compared to that suggested by BS7910 (see Table 3). In addition, it can be seen in Fig. 9(a) that the FCG trends observed in BM-A3 and BM-A4 specimens suggest that the threshold stress intensity factor range for BM in seawater is approximately $\Delta K_{th} \approx 13$ MPa√m. The near threshold data points from these two tests have been removed to identify the Paris-law constants using a simplified fit made to the linear data points, in log-log axes, in Fig. 9(b). In order to remove the deviated data points, the mean curve and upper/lower bound trends were firstly plotted for those data sets which show predominantly linear behaviour (BM-B3, BM-B4, BM-C3 and BM-C4) and then the deviated data points from BM-A3 and BM-A4 data sets which fell outside the upper and lower bound regions were omitted. The remaining data points were re-analysed to work out the power-law coefficient, C, and exponent, m, for the mean curve and upper/lower bound trends, which have been shown in Fig. 9(b) and summarised in Table 4. As seen in Fig. 9(b) and Table 4, assuming the same slope in the mean curve and upper/lower bound trends, the Paris-law coefficient and consequently the FCG rate obtained from the upper bound trend is 2.0 times higher than the mean curve for BM in seawater.

4.3. Fatigue crack growth behaviour of the HAZ material in air and seawater

The FCG data obtained from the tests performed on HAZ specimens in air and seawater are shown in Fig. 10 and Fig. 11, respectively. It can be observed in Fig. 10(a) that the FCG data for HAZ specimens in air fall upon or below the simplified Paris-law trend recommended by BS7910 for the welded joints. Note that for the range of ΔK values examined in this project ($10 < \Delta K < 50$ MPa√m) the 2-stage trend recommended by BS7910 for the assessment of welded joints is significantly higher than the simplified Paris-law trend, meaning that the FCG rates estimated by the 2-stage Paris-law are too conservative for HAZ material in air. Also seen in Fig. 10(a) is that the FCG trend in HAZ-A1 and HAZ-A2 specimens suggest that the threshold stress intensity factor range for HAZ material in air is approximately $\Delta K_{th} \approx 13$ MPa√m. The near threshold data points for these two tests which exhibit non-linearity, in log-log axes, have been removed to identify the Paris-law constants for the HAZ material in air in Fig. 10(b). To remove the deviated data points, the mean curve and upper/lower bound trends were initially plotted for those data sets which show predominantly linear behaviour (HAZ-B1, HAZ-B2, HAZ-C1 and HAZ-C2). Then the deviated data points from HAZ-A1 and HAZ-A2 data sets, which fell outside the upper and lower bound regions, were eliminated. The remaining data points were re-analysed to determine the power-law coefficient and exponent for the mean curve and upper/lower bound trends, which have been shown in Fig. 10(b) and summarised in Table 4. It can be seen in Fig. 10(b) and Table 4 that assuming the same slope in the mean curve and upper/lower bound trends, the Paris-law coefficient and consequently the FCG rate at the upper bound trend is 1.5 times higher than the mean curve for HAZ material in air.

Fig. 11(a) shows that the FCG data from the tests on HAZ material in seawater fall below the simplified and 2-stage laws recommended by BS7910 for the welded joints, closer to the simplified trend. Also seen in this figure is that similarly to the slope reduction observed for BM in seawater in Fig. 9(a), the slope of the FCG trends for HAZ-B3 and

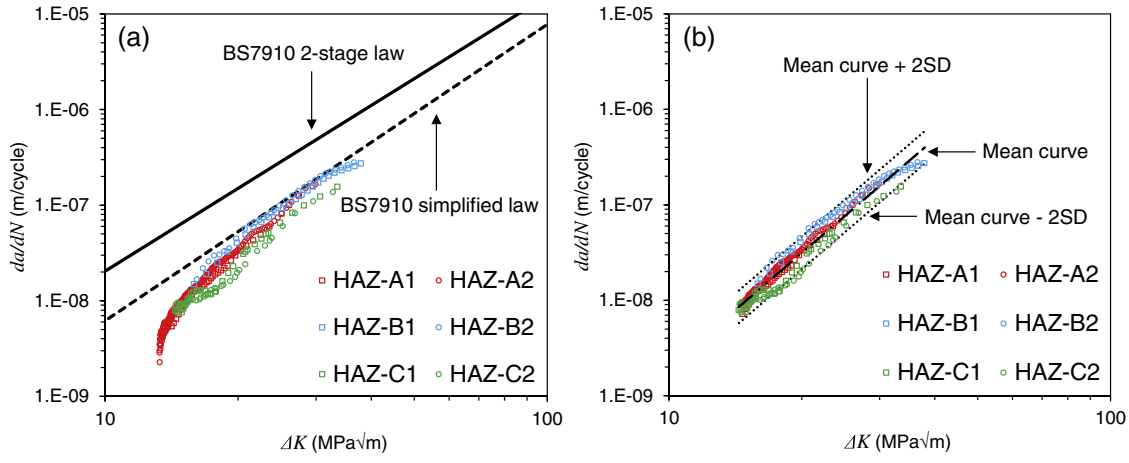

Fig. 10. FCG test data on HAZ in air (a) comparison with BS7910 recommended trends, (b) line of best fit made to the linear data points in log-log axes.

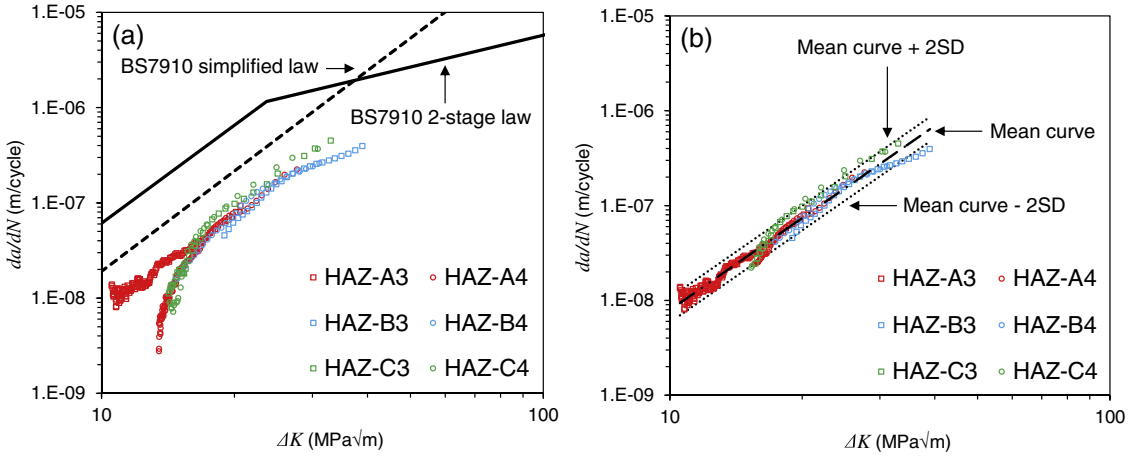

Fig. 11. FCG test data on HAZ in seawater (a) comparison with BS7910 recommended trends, (b) line of best fit made to the linear data points in log-log axes.

HAZ-B4 specimens reduces at higher values of ΔK. This figure additionally shows that the transition ΔK value at which the slope of the FCG trend changes is close to that recommended by BS7910 (see Table 3). The observed trends from all specimens apart from HAZ-A3 suggest that ΔK_{th} of the HAZ material in seawater is approximately 13 MPa√m, however it is evident from Fig. 11(a) that crack propagation was observed in the HAZ-A3 specimen at stress intensity factor ranges below 13 MPa√m. This means that 13 MPa√m cannot be taken as a conservative ΔK_{th} value for the unprotected HAZ material in seawater. The non-linear FCG data points, in log-log axes, have been removed to specify the Paris-law constants for HAZ material in seawater in Fig. 11(b). In order to remove the deviated data points, the mean curve and upper/lower bound trends were firstly plotted based on those data sets which show predominantly linear behaviour (HAZ-A3, HAZ-B3, HAZ-B4) and then the deviated data points from HAZ-A4, HAZ-C3 and HAZ-C4 data sets, which fell outside the upper and lower bound regions, were omitted. The remaining data points were re-analysed to determine the power-law coefficient and exponent for the mean curve and upper/lower bound trends, which have been shown in Fig. 11(b) and summarised in Table 4. Fig. 11(b) and Table 4 show that assuming the same slope in the mean curve and upper/lower bound trends, the Paris-law coefficient and consequently the FCG rate at the upper bound is 1.3 times higher than the mean curve for HAZ material in seawater.

4.4. Comparison of the fatigue crack growth behaviour in BM and HAZ

The mean FCG trends recommended by BS7910 for BM and welded joints in air and free-corrosion seawater environments (see Table 2 and Table 3) are presented and compared to each other in Fig. 12. In Fig. 12(a) the trends from simplified Paris-law are compared to each other whereas in Fig. 12(b) comparison has been made for 2-stage FCG trends. As seen in Fig. 12(a) and Table 2, BS7910 suggests that for a given value of ΔK, in the range of 10 to 100 MPa√m, the FCG rates in the free-corrosion environment are on average around 4 times and 5 times higher than air for BM and welded joints, respectively. A comparison of Fig. 12(a) with Fig. 12(b) shows that for $10 < \Delta K < 100$ MPa√m the simplified Paris-law recommended by BS7910 for BM provides a higher FCG trend compared to the 2-stage law, whereas for welded joints the simplified trend generally falls below the 2-stage FCG trend. Finally shown in Fig. 12(a) and Fig. 12(b) is that, depending on whether the simplified or 2-stage Paris-law recommended by BS7910 is considered in the analysis, the FCG trend in welded joints can be lower or higher than the BM for $10 < \Delta K < 100$ MPa√m.

The FCG mean curves for BM and HAZ obtained from the SLIC tests in air and seawater are presented and compared to each other in Fig. 13. The power-law constants for these mean curves can be found in Table 4. As seen in Fig. 13 and Table 4, for a given value of ΔK, the FCG rate, da/dN, is on average around 2 times higher in seawater compared

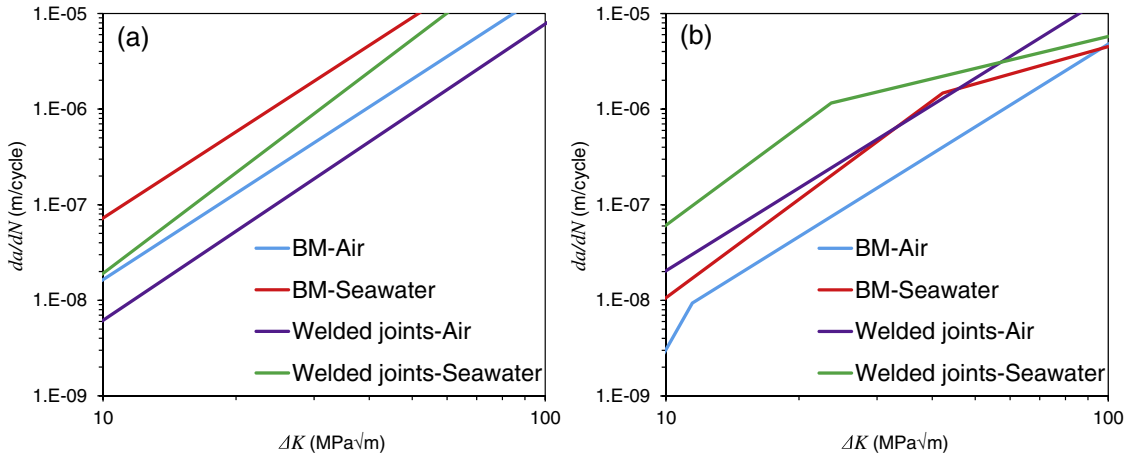

Fig. 12. Comparison of FCG trends recommended by BS7910 for BM and welded joints in air and seawater (a) simplified law (b) 2-stage law.

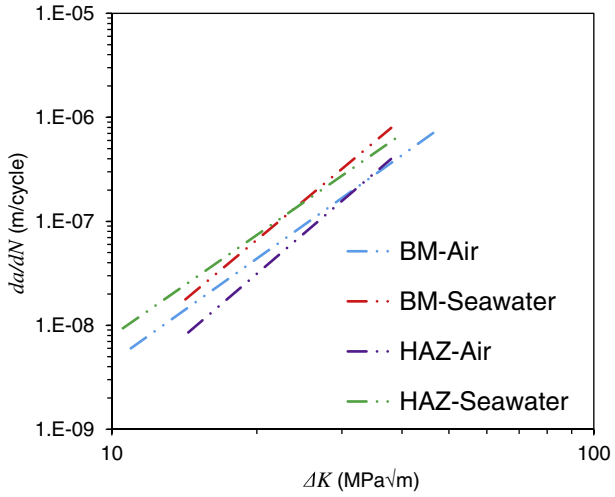

Fig. 13. Comparison of FCG mean curves for BM and HAZ in air and seawater.

to air for both BM and HAZ material. Also shown in Fig. 13 is that the mean FCG curves for BM and HAZ exhibit a similar slope of, on average, around 3.6 in air and seawater. This average slope is in good agreement with the simplified Paris-law constant, m, recommended in BS7910 for BM and welded joints in air and seawater (see Table 2). It is worth noting that although some material variability is expected within the HAZ region, it is evident that the global FCG behaviour of the HAZ material in both air and seawater environments is insensitive to the local material properties and the slope of the FCG curve is consistent with the BM. Further seen in Fig. 13 is that in both air and seawater environments the mean curves for BM and HAZ fall close to each other, particularly at higher values of ΔK.

5. Discussion

As explained earlier, the analysis of the FCG data presented above and the Paris-law constants summarised in Table 4, were based on the new shape function solution shown in Eq. (9). This equation eliminates the error encountered in shape function solutions recommended by BS ISO 12108: 2012 [23] and ASTM E647 [37] which are not accurate for shallow cracks of $a/W < 0.4$. In order to investigate the influence of inaccurate shape function solutions on the determined Paris-law constants, the results have been re-analysed using Eq. (3) and the new power-law constants in the Paris-law region are tabulated and shown in Table 5. Comparing Table 4 with Table 5 it can be seen that there are some discrepancies observed in the Paris-law constants derived from the FCG data analysed using the existing and new Y solutions (i.e. the power-law exponent generally reduces by around 0.1 when the old Y solution is employed in the analysis). Note that although the change in Y solution results in a slight change in Paris-law constants, the inaccuracies in the Y solution recommended by standards have more pronounced effects at the near threshold behaviour of the material which corresponds to shallower cracks in C(T) specimens.

It must be noted that due to the lack of residual stress measurement data on the HAZ specimens, it has been assumed that most of the welding residual stresses were released during specimen extraction from the thick welded plates. Therefore, the FCG data on HAZ specimens have been analysed using the nominal loading conditions applied on the samples and the influence of residual stresses on crack growth behaviour in C(T) specimens tested in air and seawater is assumed to be negligible. Other researchers have found that although some reduction and redistribution in residual stresses will occur when laboratory scale specimens are extracted from the welded plates [42,43], the remaining residual stresses may influence the FCG behaviour of the material, particularly in the near threshold region [44]. Therefore, residual stress measurements will be conducted on nominally identical specimens extracted from similar welded plates in future work to examine the level of residual stresses in HAZ C(T) specimens.

As previously discussed, the FCG data observed in Fig. 9 and Fig. 10 suggest that ΔK_{th} for the BM in seawater and HAZ in air is approximately 13 MPa√m which is much greater than those values recommended by BS7910 in Table 3. No values of ΔK_{th} could be inferred from other test data sets. According to BS ISO 12108: 2012 [23], $da/dN = 10^{-11}$ m/cycle is the recommended value of the FCG rate at which ΔK_{th} can be observed for most materials. For those data sets in this project that there are no experimental data available in the near threshold region, if the Paris-law trends (see Table 4) are extrapolated back to the lower ΔK region, the ΔK_{th} values corresponding to $da/dN = 10^{-11}$ m/cycle can be estimated as $\Delta K_{th} = 1.6$ MPa√m for BM in air and $\Delta K_{th} = 1.3$ MPa√m for HAZ in seawater. The obtained results from this project suggest that the ΔK_{th} values for BM and HAZ in seawater are non-zero, unlike the recommendation in BS7910 to take $\Delta K_{th} = 0$ for the free-corrosion seawater environment (see Table 3). It must be noted that the ΔK_{th} value is dependent on material properties, R-ratio, variable amplitude loading, residual stresses, test environment, crack dimensions, specimen geometry and experimental data scatter [45]. Therefore, the threshold values derived from this study may not be generalised and applied to all offshore structures.

A positive R-ratio of 0.1 was applied in all FCG tests performed in this project, even though the applied load ratio experienced by offshore wind monopile foundations may be negative. The presence of tensile residual stresses generally means that whereas a negative R-ratio might be applied, the net local stress cycle is likely to have a positive R-ratio. A review of the R-ratio effects on the FCG behaviour of steels in air and seawater shows that the FCG rates at R-ratio of −1 can be similar or lower than R = 0.1 [1,46,47]. This suggests that the FCG trends presented in this paper can be used to characterise the FCG behaviour of the offshore monopiles conservatively, however additional tests may need to be performed in future work to study the FCG behaviour of structural steel weldments at an applied $R < 0$ in more detail.

Table 5
Simplified Paris-law constants from SLIC test data (for da/dN in m/cycle and ΔK in MPa√m) using shape function solutions available in BS ISO 12108: 2012 [23] and ASTM E647 [37].

Material	Environment	Mean curve		
		C	m	R^2
BM	Air	2.83×10^{-12}	3.23	0.96
BM	Seawater (free-corrosion)	7.17×10^{-13}	3.83	0.82
HAZ	Air	2.70×10^{-13}	3.90	0.96
HAZ	Seawater (free-corrosion)	3.91×10^{-12}	3.30	0.98

6. Conclusions

Fatigue crack growth tests have been conducted on standard size BM and HAZ C(T) specimens in air, with 2 and 5 Hz cyclic frequency, and the free-corrosion seawater environment, with 0.3 Hz cyclic frequency. All air tests were performed at room temperature with the R-ratio of 0.1 and corrosion tests at 8–10 °C in standard artificial seawater. These tests were conducted at three different Test Centres as a part of the SLIC project. 24 tests were carried out in total and the following conclusions have been made from this study:

- The shape function solution recommended by standards are inaccurate for shallow cracks in a C(T) specimen geometry. Therefore, a new solution has been derived using Finite Element simulations and is presented in this paper.

- The mean curves obtained from fatigue crack growth test data show that for a given value of ΔK the FCG rate, da/dN, is on average around 2 times higher in seawater compared to air for both BM and HAZ material. This is less than the crack acceleration factor in seawater, compared to air, recommended by BS7910.
- In both air and seawater environments the mean curves for BM and HAZ fall close to each other.
- The mean fatigue crack growth curves for BM and HAZ exhibit similar slopes with an average value of 3.6, which is in good agreement with the simplified Paris-law exponents recommended in BS7910 for BM and welded joints in air and seawater.
- The ΔK_{th} value for fatigue crack growth tests on BM in seawater and HAZ in air were found to be approximately 13 MPa$\sqrt{m}$. Moreover, the test data suggest that ΔK_{th} is a non-zero value in the free-corrosion seawater environment, as opposed to the recommendation in BS7910.
- BS7910 2-stage Paris-law trends provide an acceptable estimate of fatigue crack growth behaviour for BM in air and seawater.
- BS7910 simplified Paris-law trends provide a good estimate of fatigue crack growth behaviour for HAZ in air and seawater.

Acknowledgements

The authors would like to acknowledge the help and contribution of the SLIC steering committee, project technical support team, fabricators, specimen manufacturers, Test Centres and other members of the technical delivery team at Cranfield University. This work was supported by EPSRC under Grant EP/L016303/1 (Renewable Energy Marine Structures (REMS) Centre for Doctoral Training).

References

[1] O. Adedipe, F. Brennan, A. Kolios, Review of corrosion fatigue in offshore structures: Present status and challenges in the offshore wind sector, Renew. Sustain. Energy Rev. 61 (2016) 141–154.
[2] Engineering Sciences Data Unit, Fatigue crack propagation in low and medium strength low alloy steel plate, bar and forgings, London: ESDU Data Sheet 81, 011, 1981.
[3] N.E. Frost, K.J. Marsh, L.P. Pook, Metal Fatigue, Courier Corporation, 1974.
[4] C.M. Hudson, S.K. Seward, A compendium of sources of fracture toughness and fatigue-crack growth data for metallic alloys, Int. J. Fract. 14 (1978) R151–R184.
[5] C.M. Hudson, S.K. Seward, A compendium of sources of fracture toughness and fatigue crack growth data for metallic alloys - part II, Int. J. Fract. 20 (1982) R59–R117.
[6] C.M. Hudson, S.K. Seward, A compendium of sources of fracture toughness and fatigue crack growth data for metallic alloys — part III, Int. J. Fract. 39 (1989) R43–R63.
[7] C.M. Hudson, J.J. Ferrainolo, A compendium of sources of fracture toughness and fatigue crack growth data for metallic alloys-part IV, Int. J. Fract. 48 (1991) R19–R43.
[8] Underwater Engineering Group, Design of tubular joints for offshore structures, London: UR33, 1985.
[9] D. Taylor, A Compendium of Fatigue Thresholds and Growth Rates, 1985, Engineering Materials Advisory Services, 339 Halesowen Road, Cradley Heath, Warley, West Midlands B 64 6PH, UK, 1985 380.
[10] C. Jaske, J. Payer, V. Balint, Corrosion fatigue of metals in marine environments, DTIC Document, 1981.
[11] I. Austen, E. Walker, Corrosion fatigue crack growth rate information for offshore life prediction, Steel in Marine Structures–SIMS' 87 1987, pp. 859–870.
[12] G. Booth, S. Dobbs, Corrosion fatigue crack growth in BS 4360 Grade 50D steel, Weld. Inst. Res. Bull. 27 (1986) 293–297.
[13] A. McEvily Jr., Atlas of Stress-Corrosion and Corrosion Fatigue Curves, 1990.
[14] S. Suresh, R.O. Ritchie, On the influence of environment on the load ratio dependence of fatigue thresholds in pressure vessel steel, Eng. Fract. Mech. 18 (1983) 785–800.
[15] R. Ritchie, Near-threshold fatigue crack propagation in ultra-high strength steel: influence of load ratio and cyclic strength, J. Eng. Mater. Technol. 99 (1977) 195–204.
[16] R. King, A review of fatigue crack growth rates for offshore steels in air and seawater environments, HSE Report OTH 511, Health & Safety Executive Books, London, 1998.
[17] S.J. Garwood, Fatigue crack growth threshold determination; a simple estimation technique, Weld. Inst. Res. Bull. 20 (1979) 262–265.
[18] R. Ritchie, Near-threshold fatigue-crack propagation in steels, Int. Metals Rev. 24 (1979) 205–230.
[19] A.T. Stewart, The influence of environment and stress ratio on fatigue crack growth at near threshold stress intensities in low-alloy steels, Eng. Fract. Mech. 13 (1980) 463–478.
[20] I. Austen, Measurement of fatigue crack threshold values for use in design, BSC Report SH/EN/9708/2/83/B, 1983.
[21] Guide on Methods for Assessing the Acceptability of Flaws in Fusion Welded Structures, BSI, London, 2013.
[22] F. Brennan, I. Tavares, Fatigue design of offshore steel mono-pile wind substructures, Proc. Inst. Civ. Eng. Energy 167 (2014) 196–202.
[23] BS. ISO 12108, Metallic Materials — Fatigue Testing — Fatigue Crack Growth Method, British Standards Institution, London, 2012 2012.
[24] BS. 3518-3, Methods of Fatigue Testing —Part 3: Direct stress fatigue tests, British Standards Institution, London, 1963 1963.
[25] BS. 3518-1, Methods of Fatigue Testing — Part 1: Guide to General Principles, British Standards Institution, London, 1993 1993.
[26] BS. ISO 12108, Metallic Materials — Mechanical Testing — Vocabulary, British Standards Institution, London, 2007 2007.
[27] BS. ISO 4965-2, Metallic Materials — Dynamic Force Calibration for Uniaxial Fatigue Testing Part 2: Dynamic Calibration Device (DCD) Instrumentation, British Standards Institution, London, 2012 2012.
[28] BS. ISO 23788, Metallic Materials — Verification of the Alignment of Fatigue Testing Machines, British Standards Institution, London, 2012 2012.
[29] ASTM. D1141-98, Standard Practice for the Preparation of Substitute Ocean Water. Annual Book of ASTM Standards, 2008, ASTM International, 2008.
[30] BS. EN ISO 11782-2, Corrosion of metals and alloys — Corrosion fatigue testing — Part 2: Crack propagation testing using precracked specimens, British Standards Institution, London, 2008 2008.
[31] O. Adedipe, F. Brennan, A. Kolios, Corrosion fatigue load frequency sensitivity analysis, Mar. Struct. 42 (2015) 115–136.
[32] S. Dhinakaran, R.V. Prakash, Effect of low cyclic frequency on fatigue crack growth behaviour of a Mn–Ni–Cr steel in air and 3.5% NaCl solution, Mater. Sci. Eng. A 609 (2014) 204–208.
[33] Y.-S. Shih, J.-J. Chen, The frequency effect on the fatigue crack growth rate of 304 stainless steel, Nucl. Eng. Des. 191 (1999) 225–230.
[34] A.R. Henderson, M.B. Zaaijer, Hydrodynamic loading on offshore wind turbines, The Fourteenth International Offshore and Polar Engineering Conference, International Society of Offshore and Polar Engineers, 2004.
[35] T.L. Anderson, Fracture Mechanics: Fundamentals and Application, CRC Press, Boston, 1991.
[36] H. Tada, P.C. Paris, G.R. Irwin, The Stress Analysis of Cracks Handbook, Paris Productions & (Del Research Corp.), Saint Louis, 1985.
[37] ASTM. E 647-13, Standard Test Method for Measurement of Fatigue Crack Growth Rates. Annual Book of ASTM Standards, 2008.
[38] P.C. Paris, F. Erdogan, A critical analysis of crack propagation laws, J. Basic Eng. 85 (1960) 528–534.
[39] A. Mehmanparast, C.M. Davies, D.W. Dean, K.M. Nikbin, The influence of pre-compression on the creep deformation and failure behaviour of type 316H stainless steel, Eng. Fract. Mech. 110 (2013) 52–67.
[40] J.E. Srawley, Wide Range Stress Intensity Factor for ASTME399 Standard Fracture Toughness Specimens, Int. J. Fract. 12 (1976) 475–476.
[41] ABAQUS, User Manual. in Version 6.13 ed: in Version 6.13, SIMULIA, 2013.
[42] G. Pouget, A.P. Reynolds, Residual stress and microstructure effects on fatigue crack growth in AA2050 friction stir welds, Int. J. Fatigue 30 (2008) 463–472.
[43] S. Lewis, S. Hossain, D. Smith, C. Truman, M. Hofmann, Determination of remnant residual stresses in fracture toughness specimens extracted from large components, Strain 47 (2011).
[44] R. John, K.V. Jata, K. Sadananda, Residual stress effects on near-threshold fatigue crack growth in friction stir welds in aerospace alloys, Int. J. Fatigue 25 (2003) 939–948.
[45] U. Zerbst, M. Vormwald, R. Pippan, H.-P. Gänser, C. Sarrazin-Baudoux, M. Madia, About the fatigue crack propagation threshold of metals as a design criterion – a review, Eng. Fract. Mech. 153 (2016) 190–243.
[46] T.W. Thorpe, P.M. Scott, A. Rance, D. Silvester, Corrosion fatigue of BS 4360:50D structural steel in seawater, Int. J. Fatigue 5 (1983) 123–133.
[47] O. Adedipe, F. Brennan, A. Kolios, A relative crack opening time correlation for corrosion fatigue crack growth in offshore structures, Fatigue Fract. Eng. Mater. Struct. (2015).